Journal of
Mechanics of
Materials and Structures

THE STRESS-MINIMIZING HOLE IN AN ELASTIC PLATE UNDER REMOTE SHEAR

Shmuel Vigdergauz

Volume 1, Nº 2 February 2006

mathematical sciences publishers

JOURNAL OF MECHANICS OF MATERIALS AND STRUCTURES
Vol. 1, No. 2, 2006

THE STRESS-MINIMIZING HOLE IN AN ELASTIC PLATE UNDER REMOTE SHEAR

SHMUEL VIGDERGAUZ

Conformal mappings provide an elegant formulation for planar elastostatic problems. Here, the mapping function coefficients are used in a new manner as design variables in the genetic-algorithm (GA) approach to find a piecewise smooth optimal shape of a single traction-free hole in an elastic plate that minimizes the local stresses under remote shear. This scheme is sufficiently fast and accurate to numerically show that the sought-for shape generates tangential stress of constant absolute value, equal to 30% less than the stress concentration factor (SCF) for the commonly used circular hole. The shape has four symmetrically located corners, and the stress changes sign while remaining finite as it rounds each corner. This is the same shape as the energy-minimizing contour identified in 1986 by the author and Cherkaev for the same load. Other nontrivial examples are given to demonstrate the potential of the approach. Methodologically, this article continues the optimization study first conducted by the author and Cherkaev (*J. Appl. Math. Mech.* **50**:3 (1986), 401–404) and subsequently by Cherkaev et al. (*Internat. J. Solids Structures* **(35)**:33, 4391–4410).

1. Introduction

Designing elastic structures to diminish the stresses around construction holes in flat plates remains an actual problem in spite of intensive studies carried out in the area over the last decades. Various stress-reducing technologies, such as auxiliary unloading holes, reinforcement rings and others are known so far, each posing its own elastostatic problem. In most applications, the hole area matters much more than its shape, which thus permits a certain freedom in design. Prompted by this, our concern here is with optimization of the hole shapes to minimize the stress concentration factor (SCF), denoted by $\mathcal{H}$, and defined as the maximum modulus of the tangential stress along the holes, at unit remote load. The lesser the factor, the stronger the hole-weakened construction will be. Technologically, only piecewise smooth holes with a finite number of corner points may be used as stress-minimizers. This is assumed in what follows.

Keywords: plane elasticity problem, Kolosov–Muskhelishvili potentials, shape optimization, effective energy, extremal elastic structures, genetic algorithm.

The SCF, though local in nature, is obtainable only from full-scale elastic stress solutions, which are rarely known in a closed form. A nontrivial example is a uniform stress distribution

$$\sigma_{\tau\tau} = \text{Const} \tag{1}$$

occurring at specifically shaped interfaces [Cherepanov 1974]. Here τ stands for the contour unit tangent. These equistress shapes do exist in an infinite plane in any number and mutual arrangement, provided the remote deviatoric load is relatively small, as stated accurately in the next section. In particular, pure bulk gives $\mathcal{K} = 2$ independently of the geometry of the hole set. The equistress condition not only prevents the stress concentration at the hole but also provides the global minimum of $\mathcal{K}$ over all shapes at given bulk-type loading [Vigdergauz 1976].

In the opposite case of pure shear, the $\mathcal{K}$-optimal shapes are yet unknown, even for the simplest configuration of a single traction-free hole. To make progress in this stubborn problem, we replaced the local criterion $\mathcal{K}$ in [Vigdergauz and Cherkayev 1986] by the less severe global criterion of minimizing the hole-induced energy perturbation δW, taken at unit load and related to the hole area. In the effective medium theory, a minimum in δW corresponds to maximum shear rigidity of a dilute planar composite when the holes are far apart and have little influence on each other (see [Torquato 2002], for instance). Derived variationally, this optimality condition then implies constancy of the *absolute* value of the tangential stresses along the sought-for contour

$$|\sigma_{\tau\tau}| = \text{Const}. \tag{2}$$

In contrast to the equistress condition (1), the less restrictive identity (2) may be compatible with remote shear load, provided the stresses change sign across a finite number of angular points. Using this assumption, the resultant near-square hole shape is found numerically [Vigdergauz and Cherkayev 1986] with $\delta W = 3.714\ldots$.

Conversely, (2) is an immediate result of (1); hence equistress $\mathcal{K}$-optimal shapes, when they exist, also minimize the energy perturbation δW under a fixed load.

Though similar, identities (1) and (2) work differently. The second one is used as a prerequisite in directly finding the energy-minimizing shapes at any far load (see details in [Cherkaev et al. 1998]), while $\mathcal{K}$-optimality of the equistress condition (1) is revealed only *a posteriori* [Vigdergauz 1976]. The proof is based on the maximum module principle, which is not applicable to the shear-type stress field associated with (2). This brings up the following inverse problem:

Among all possible continuous curves, find the shape of a single hole in an elastic plate so as to minimize the factor $\mathcal{K}$ under pure shear at infinity.

The challenge is very interesting mathematically, and its practical importance is in providing the theoretical bound of material behavior. The latter is significant to the designer, who can determine how far the actual structure is from the theoretical optimum. As excellent sources on the direct problem of finding $\mathcal{K}$ for various shapes, we refer to the classical monograph [Savin 1961] and the recently reprinted [Pilkey 1997].

In the absence of the $\mathcal{K}$-optimal precondition, semianalytical and numerical global optimization are the methods of choice in solving the problem. The purpose of this paper is twofold: to present a new numerical optimization scheme, and to produce new optimal solutions not available in the literature.

Computationally, any optimization process involves two main ingredients: the solution of a given direct boundary value problem, which has to be repeated many times, and a minimization scheme. As the first ingredient, we choose the Kolosov–Muskhelishvili potentials $\varphi(z)$ and $\psi(z)$ [Muskhelishvili 1963], together with the conformal mapping of the sought-for contour onto a circle. Thanks to the power of complex variable techniques, this combination provides an effective numerical solver of the direct problem. Especially relevant here is the scheme by Kalandiya [1975], in which the contour stresses are solved from an infinite system of linear algebraic system with easy-to-compute coefficients. In practice, the system size and the Laurent series expansion of the mapping function are both truncated at different finite orders. We have substantially improved the algorithmic performance of the scheme in the following two aspects. First, we show that a finite mapping expansion generates *exactly* a finite-size system, thus allowing to avoid the additional truncation error. Second, the analytical manipulations over $\sigma_{\tau\tau}$ are performed to the maximum extent resulting in a simple rational expression. The latter provide evaluation of the local-type function $\mathcal{K}$ with sufficient accuracy to be incorporated into the genetic algorithm (GA) optimization process rapidly gaining use in elasticity. For design variables we choose coefficients of the mapping function instead of the contour nodal points, used in [Vigdergauz 2001b; 2001a; 2002]. This drastically reduces the number of design variables and allows the analytic calculation of all the integrals that occur. On this basis, the energy-minimizing shapes (2) are numerically shown to remain $\mathcal{K}$-optimal under pure shear as in the equistress case (1) under bulk load. We also calculate the energy-maximizing holes for a small number of mapping coefficients, to illustrate the "worst" possible situation.

In Section 2 we recall basic facts of complex variable theory applied to plane elasticity. Section 3 states the optimization problem and details the mixed GA/conformal mapping solving technique. Section 4 details the novel scheme of evaluating tangential stresses along the hole shape. Numerical comparison with the less accurate approach of Cherkaev et al. [1998] is performed in Section 5. Some analytical consequences are deduced in Section 6. They serve as a benchmark

for GA testing and calibration (Section 7). The numerical results are given and discussed in Section 8. Section 9 contains some final remarks.

2. The Kolosov–Muskhelishvili approach in plane elasticity

Consider the setup in Figure 1. Let an infinite elastic plane E be weakened by a hole with a piecewise smooth boundary L enclosing the origin of xy-plane. The curve L divides the plane in the hole region S_1 of finite area f_1 and the outside region $S_2 = E \setminus S_1$, filled with a linearly elastic phase. Let the plate be remotely loaded by uniform nontangential stresses

$$\sigma_{xx}^0 = P, \quad \sigma_{yy}^0 = Q, \quad \sigma_{xy}^0 = 0. \tag{3}$$

Let S_2 be conformally mapped onto the exterior Σ_2 of the unit circle Σ_1 with the boundary l in the auxiliary plane $F = \Sigma_1 \cup \Sigma_2$ of the complex variable ζ. Up to a scaling factor, the mapping function $\omega(\zeta) : S_2 + L \to \Sigma_2 + l$ is represented as a

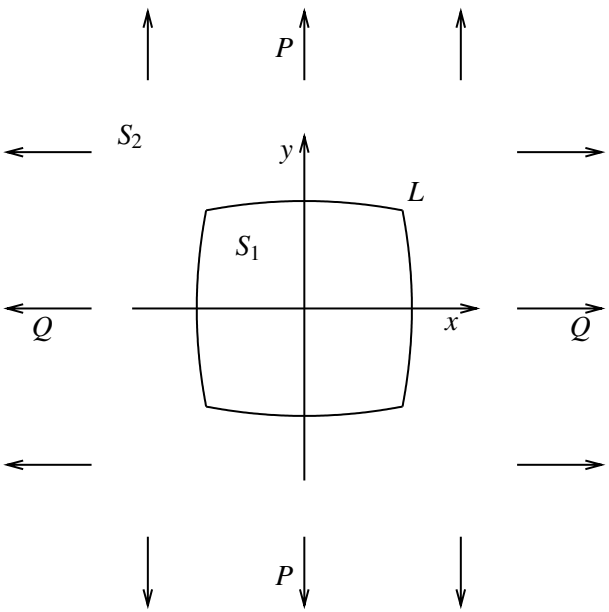

Figure 1. An infinite plate with a traction-free hole under uniform stresses. The cases $P = Q$ and $P = -Q$ correspond to remote bulk and shear, respectively. The piecewise smooth boundary of the hole has a certain rotational symmetry and possibly a finite number of corners.

Laurent series

$$\omega(\zeta) = \zeta + \sum_{k=1}^{\infty} d_k \zeta^{-k}, \tag{4}$$

with

$$f_1 = \pi\left(1 - \sum_{k=1}^{\infty} k|d_k|^2\right). \tag{5}$$

(See [Ahlfors 1978] for this and subsequent background facts from complex function theory.) Since the map $\omega(\zeta)$ must be one-to-one, its coefficients fall in the intervals

$$-\frac{1}{\sqrt{m}} \le d_m \le \frac{1}{\sqrt{m}}, \quad m = 1, 2, \ldots. \tag{6}$$

The Airy stress function remains biharmonic under the map and hence is expressed through the Kolosov–Muskhelishvili (KM) potentials $\Phi_0(\zeta)$, $\Psi_0(\zeta)$, analytic in Σ_2 [Muskhelishvili 1963], with far field asymptotics governed by (3):

$$\Phi_0(\zeta) = B + \Phi(\zeta), \ \Psi_0(\zeta) = \Gamma + \Psi(\zeta); \ \ \zeta \in \Sigma_2, \quad \Phi(\zeta), \ \Psi(\zeta) = O\left(|\zeta|^{-2}\right), \tag{7a}$$

$$4B = Q + P, \ \ 2\Gamma = Q - P, \quad \operatorname{Im} B = \operatorname{Im} \Gamma = 0. \tag{7b}$$

As in (4), they also have convergent series expansions (the summation begins with $n = 2$ to match the asymptotics (7a)):

$$\Phi(\zeta) = \sum_{k=2}^{\infty} a_k \zeta^{-k}, \quad \Psi(\zeta) = \sum_{k=2}^{\infty} b_k \zeta^{-k}; \qquad \zeta \in \Sigma_2 + l, \tag{8}$$

with (see for instance Vigdergauz [2001b])

$$\delta W = 2\pi f_1^{-1}\left(2\Gamma a_2 + B b_2\right). \tag{9}$$

For simplicity, suppose that the hole boundary is traction-free. Then the stresses $\sigma_{\varrho\varrho}(\xi)$ and $\sigma_{\varrho\theta}(\xi)$ vanish along it: $\xi = \exp i\theta$, $\varrho = 1$ in the plane F, thus forming the boundary condition for the KM potentials

$$-\frac{2}{\xi^2}\overline{\omega'(\xi)}\operatorname{Re}\Phi_0(\xi) + \overline{\omega(\xi)}\Phi_0{}'(\xi) + \omega'(\xi)\Psi_0(\xi) = 0; \quad \xi \in l. \tag{10}$$

The nonzero stress component $\sigma_{\tau\tau}(t(\xi)) \equiv \sigma_{\theta\theta}(\xi)$ along l possesses the form [Muskhelishvili 1963]

$$\sigma_{\theta\theta}(\xi) = 4Re\Phi_0(\xi) = 4B + 4\sum_{k=2}^{\infty} a_k \cos(k\theta); \quad \xi \in l. \tag{11}$$

Of course, the stresses and strains at any point inside Σ_2 are also expressed in $\Phi_0(\zeta)$, $\Psi_0(\zeta)$ [Muskhelishvili 1963]. We omit the formulas here to save room.

Identities (7) and (10) form the boundary value problem in the KM potentials. This problem is uniquely solvable [Muskhelishvili 1963], at least for any piecewise smooth inclusion shape L, which is therefore the only factor defining the problem's solving complexity. Specifically, the equistress principle (1) yields $\sigma_{\varrho\theta}(\xi) = 4B$, and hence (see [Cherepanov 1974])

$$\Phi_0(\zeta) = B, \quad \omega(\zeta) = \zeta - \kappa\zeta^{-1}, \quad \omega'(\zeta)\Psi_0(\zeta) = -B\frac{\kappa\zeta^2 + 1}{\zeta^2 + \kappa}; \quad \kappa \equiv \frac{\Gamma}{2B}.$$

The equistress shape appears to be an ellipse that exists if and only if

$$|\kappa| \equiv |d_1| < 1,$$

or equivalently, thanks to (3) and (7b),

$$\sigma^0_{xx}\sigma^0_{yy} \geq 0.$$

3. Problem reformulation, design variables and basic GA scheme

In contrast, under the shear-dominated far field (3) when $\sigma^0_{xx}, \sigma^0_{yy}$ are of opposite signs, the $\mathcal{K}$-optimal hole shape cannot be found in a closed form. Thus, numerical methods are called for. In computational practice, the expansion (4) is necessarily truncated at a finite number N of first terms. With this in view, our optimization problem is reformulated as follows:

At a given finite number N of mapping coefficients and pure shear field $B = 0$, find the $\mathcal{K}$-optimal hole shape on which

$$\mathcal{K} \equiv \max_{t\in L_N} |\sigma_{\tau\tau}(t)| \equiv \max_{\xi\in l} |\sigma_{\theta\theta}(\xi)| \xrightarrow[\{L_N\}]{} \min, \tag{12}$$

where $\{L_N\}$ denotes the set of all curves mapped onto the unit circle by $\omega(\zeta)$ with any admissible finite set $\{d_m,\ m = 1, \ldots, N\}$, and $d_m = 0, m > N$.

In our opinion, the N-parametric nonlinear optimization problem (12) with the linear restrictions (6) is well suited to be solved by the genetic algorithm advanced in [Holland 1975]. This heuristic method performs a nongradient stochastic search for the global optimum by mimicking the Darwinian principal of survival of the fittest through blind mutation and natural selection over successive generations; see [Gen and Cheng 1997] for a state-of-the-art review and many references. GA specifics, as applied to shape optimization in planar elasticity, are illustrated in [Vigdergauz 2001b; 2001a; 2002] where the radii of nodal points equally spaced along the sought-for contour are directly taken as the GA design variables without a conformal premapping. This scheme helps find the δW-optimal hole shapes, but is not sufficiently accurate to handle the local criterion $\mathcal{K}$. For this reason, optimized contours are represented here through a set of mapping coefficients rather than through nodal points. This not only dramatically reduces the number of required

design variables but also allows the development of an efficient fitness evaluation scheme (see the next sections) which is easily included into a standard GA configuration.

On the other hand, in contrast to the nodal-based shape encoding, a mapped contour may have self-intersections even assuming inequalities (6) on the mapping coefficients. Other uniqueness conditions imply that all the roots of the polynomial $P_{N+1}(\zeta) = \zeta^{N+1}\omega'(\zeta)$ lie strictly inside the unit circle (see [Ahlfors 1978]):

$$P_{N+1}(\zeta) = \zeta^{N+1} - \sum_{m=1}^{N} m d_m \zeta^{N-m} = \prod_{m=1}^{N+1} (\zeta - \lambda_m); \qquad |\lambda_m| < 1, \quad m = 1, \ldots, N+1. \tag{13}$$

Though more restrictive than (6) these bounds are also only necessary but not sufficient to avoid self-intersections. Mathematically, this is because for $N > 1$, such inequalities provide a one-to-one mapping only locally rather than globally, as exemplified in Figure 2, where the mapping terms are strictly inside the intervals (6).

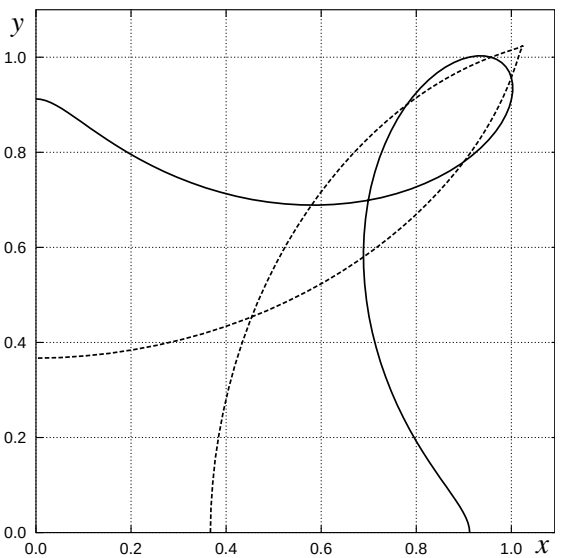

Figure 2. Two-term conformal mapping of the unit circle onto a self-crossing line with square symmetry: $d_3 \approx 0.24451093$, $d_7 \approx 0.15696709$, the largest root modulus is approximately 1.47730100 is outside the circle (the solid line), and $d_3 \approx -0.54182861$, $d_7 \approx -0.09122962$, with all the roots inside the circle (the dotted line). The loop areas enter identity (5) with a negative sign.

To exclude self-intersections, we use the geometric fact that a closed curve

$$\omega(\xi) = \rho(\xi) \exp i\vartheta(\xi), \quad \xi = \exp i\theta \in l, \tag{14}$$

with p-fold rotational symmetry is intersection-free if and only if $\vartheta(\xi)$ is an increasing function of θ in the interval $0 < \theta < \pi/p$. Though seemingly cumbersome, this condition is quickly checked over a discrete set of points along the irreducible part of mapped curves with penalizing their fitness to the extent by which (14) is violated at the first point so detected.

(We note in passing that the nonmonotony of finite-term mappings produces a closed loop of a negative area. This formally results in zero-area curves with self-intersections rather than in physically reasonable zero-area slits. The trivial exception is the case $p = 1$, when the function $\omega(\zeta) = \zeta + \zeta^{-1}$ maps the unit circle to a rectilinear slit

$$L : -2 \le t \le 2$$

at the x-axis of the physical plane E. In Section 8 this note is used to explain the numerically found behavior of the energy-maximizing hole shapes.)

Another difficulty of the proposed scheme is that a relatively small number N of mapping coefficients smoothes the shape corners and hence may yield too conservative an optimum. However, it is physically clear that the stresses should be bounded at the "true" corners of the optimal shape, which makes only an infinitely small contribution to the minimized criterion value. Earlier work [Vigdergauz and Cherkayev 1986] and our current results show that this is the case.

4. Fast stress-evaluation scheme

We now refer back to the direct boundary problem (7), (10), the solution of which gives the value of $\mathcal{H}$ for an arbitrarily shaped hole. Our concern here is to maximally extend the analytical transformations before resorting to numerical calculations. To this end, we rework the boundary condition (10) with (7a) as

$$-\frac{2B}{\xi^2}\overline{\omega'(\xi)} + \Gamma\omega'(\xi) - \frac{2}{\xi^2}\overline{\omega'(\xi)}\,\mathrm{Re}\,\Phi(\xi) + \overline{\omega(\xi)}\Phi'(\xi) = -\omega'(\xi)\Psi(\xi); \quad \xi \in l. \tag{15}$$

The left-hand side of (15) is the boundary value of an Σ_2-holomorphic function tending to zero at infinity. In turn, this means that its series expansion involves no nonnegative powers in ζ. Substituting (4) and (8) in (15) and zeroing the resulting coefficients of ζ^n, $n \ge 0$, gives an infinite linear algebraic system in a_k, $k \ge 2$:

$$a_{m+2} - \sum_{k=1}^{m}(m-k+1)\bar{d}_{m-k+1}a_k - (m+1)\sum_{k=1}^{\infty}\bar{d}_{m+k+1}\bar{a}_k = A_m; \quad m = 0, 1, \ldots, \tag{16a}$$

$$A_0 = 2B - \Gamma, \quad A_1 = 0, \quad A_m = -2B(m+1)\bar{d}_{m+1}, \quad m \ge 2. \tag{16b}$$

The first sum is omitted in (16a) when $m = 0, 1$.

Remarkably, the second potential $\Psi(\zeta)$ remains outside the system, thus allowing us to separate out the coefficients a_k, which are only needed to compute the boundary stresses $\sigma_{\theta\theta}(\xi)$ via (11). In numerical practice, the mapping expansion (4) and the system size are truncated to finite numbers.

This scheme was proposed by Kalandiya [1975] three decades ago and since then, to the author's best knowledge, it has not yet been studied analytically. Our aim now is to prove that the double truncation is unnecessary, because by taking only the N first items in the mapping expansion (4) the actual system size already shrinks to the same finite value of N.

To make the algebra simpler, assume that the unit far field is only shear ($B = 0$, $\Gamma = 1$) and that the hole shape L is symmetric about the x-axis. Then the coefficients $\{a_k, b_k, d_k\}$ are real and hence

$$\delta W = \pi a_2 f_1^{-1}. \tag{17}$$

Independently of these assumptions, we further note that with $d_n = 0$, $n > N$ the second sum disappears in all equations (16a) from $m = N - 1$ on. Beginning with $m = N$ they form an infinite linear system of finite differences

$$a_{m+2} - \sum_{k=1}^{N} k d_k a_{m-k+1} = 0; \qquad m = N,\ N+1, \ldots, \tag{18}$$

with constant coefficients $1, 0, -d_1, -2d_2, \ldots, -Nd_N$ which define the finite Laurent expansion of $\omega'(\zeta)$. For this reason, the characteristic roots of (18) coincide with the set of roots $\{\lambda_k\}$ of (13); see [Levy and Lessman 1958]. This is the key point for further analysis.

Suppose first that all the roots of $P_{N+1}(z)$ are different. Then the general solution to the homogeneous system (18) takes the form

$$a_m = D_1 \lambda_1^m + D_2 \lambda_2^m + \ldots + D_{N+1} \lambda_{N+1}^m, \quad m = 1, 2, \ldots, \tag{19}$$

where the arbitrary constants $D_1, \ldots, D_{N+1}$ are to be found by plugging (19) into (16). Substitution of (19) into (8) results in infinite geometrical progressions in ζ, which converge by virtue of inequalities (13). Summing them we get, in view of (13),

$$\Phi(\zeta) = \sum_{m=1}^{N+1} \frac{D_m \lambda_m^2}{\zeta(\zeta - \lambda_m)}. \tag{20}$$

In order to avoid the polynomial roots calculation, we exclude them by performing summation in (20) over m:

$$\Phi(\zeta) = \frac{R_N(\zeta)}{\zeta \omega'(\zeta)}. \tag{21}$$

Here $R_N(\zeta)$ is a new polynomial of degree N in ζ,

$$R_N(\zeta) = r_N \zeta^N + r_{N-1} z^{N-1} + \ldots + r_0. \tag{22}$$

It is easy to see that the coefficients r_m, $m = 0, \ldots, N$ are specified by

$$r_m = (-1)^m \sum_{j=1}^{N+1} D_j \lambda_j p_m^j, \tag{23}$$

where p_m^j stands for all the possible products of m different roots λ_k excluding λ_j and $p_0^j \equiv 1$.

Writing out p_m^j through the coefficients (13) of the polynomial $P_{N+1}(\zeta)$ and making use of (19) we obtain finally

$$\begin{aligned} &r_0 = a_1 = 0, \qquad r_1 = a_2, \\ &r_m = a_{m+1} + \sum_{j=1}^{m-1} (-1)^{m-j} (m - j + 1) d_{m-j+1} a_j; \qquad m \geq 2. \end{aligned} \tag{24}$$

Therefore, the net expression (21) for the potential $\Phi(\zeta)$ does not explicitly contain the roots λ_m. Lastly, the second potential $\Psi(\zeta)$ is algebraically found from (15).

For the multiple roots λ_m, analogous manipulations lead to the same formulas, (21) and (24). Note that the s-repeated root λ_m enters expression (19) for a_m as

$$D_k^1 \lambda_k + k D_k^2 \lambda_k^2 + \ldots + D_k^{s-1} \lambda_k^s; \tag{25}$$

see [Levy and Lessman 1958]. Substitution of (25) into (8) results in convergent sums of the type

$$S_m = \sum_{i=1}^{m} i^m x^i, \qquad |x| < 1,$$

which are found recurrently. Indeed, it is evident that $S_0 = x(1-x)^{-1}$, while for $m \geq 1$,

$$S_m = \frac{x}{1-x} \left(1 + \sum_{j=1}^{m-1} \binom{m}{j} S_j \right),$$

as follows from the chain of identities

$$S_m = \sum_{i=1}^{m} i^m x^i = x + \sum_{i=1}^{m} (i+1)^m x^{i+1} = x + x \sum_{j=1}^{m} \binom{m}{j} S_j.$$

Further simplification is made by assuming a possible stress field symmetry which permits the unknowns to be partially eliminated. Say, for a square-symmetric hole ($d_k = 0$ when $k \neq 4j - 3$) and pure shear, only a_{4k-2}, $k = 1, 2, \ldots$, differ from zero.

5. Comparison with the truncated expansion solution

For clarity, we repeat the basic steps of the proposed evaluation scheme.

First, the map function (4) is assumed to contain only a finite number N of terms.

Next, the linear algebraic system of the first N equations from (16) is solved to find the N lowest coefficients of $\Phi(\zeta)$. We remark again that the higher coefficients do not enter the system, which hence is *exact* with no truncation needed. The first term a_2 so found gives the energy increment δW via (9). The more general energy-related Pólya–Szegő matrices are derived in [Movchan and Serkov 1997] exactly in this way.

The final and novel component is finding the function $\Phi(\zeta)$ or, equivalently, the tangential stress distribution $\sigma_{\theta\theta}(\xi)$ along the hole shape by the exact summation of the infinite tail in expansion (8). This is not done in [Cherkaev et al. 1998], where the truncated series

$$\Phi(\zeta) = \sum_{k=2}^{N} a_k \zeta^{-k} \tag{26}$$

is used instead. This brings up the question of assessing the resultant truncation error in the local stresses in dependence on N. To this end we borrow the δW-optimal mapping terms for $n = 3, 7, 11, 15$ found in [Cherkaev et al. 1998] for square symmetry and use (22)–(24) and (26) to compute the exact and truncated $\mathcal{K}$. At a given $\{d_k\}$ (Table 1), the discrepancy between the values (Table 2) is entirely due to the system truncation. The relative error $\Delta\mathcal{K}$ is seen to decrease rather slowly with increasing N. In addition, the truncation leads to spurious oscillations as exemplified in Figure 3 for $N = 23$. This validates the proposed $\mathcal{K}$-evaluation scheme against (26).

N	d_3	d_7	d_{11}	d_{15}	d_{19}	$\delta W_{\min}$
3	−0.13807					3.72792
7	−0.14251	0.01575				3.71725
11	−0.14372	0.01652	−0.00513			3.71532
15	−0.14420	0.01683	−0.00539	0.00239		3.71473
19	−0.14445	0.01699	−0.00521	0.00251	−0.00134	3.71449

Table 1. A single square-symmetric hole under remote shear: the optimal mapping coefficients and the global criterion $\delta W_{\min}$ for different values of N, taken from [Cherkaev et al. 1998].

	Exact Summation		Truncation		
N	value	angle	value	angle	$\Delta\mathcal{H}(\%)$
3	3.29603	31.5	3.51472	0.0	6.63
7	3.26002	37.3	3.32372	22.9	1.95
11	3.25179	39.6	3.29671	30.3	1.38
15	3.24801	40.9	3.28945	34.0	1.27
19	3.24623	41.6	3.28690	36.3	1.25

Table 2. Values of $\mathcal{H}$ and angular locations along the δW-optimal hole shape, under exact summation (Eqs. (22)–(24)) and under truncation (Eq. (26)). See Table 1 for the mapping coefficients.

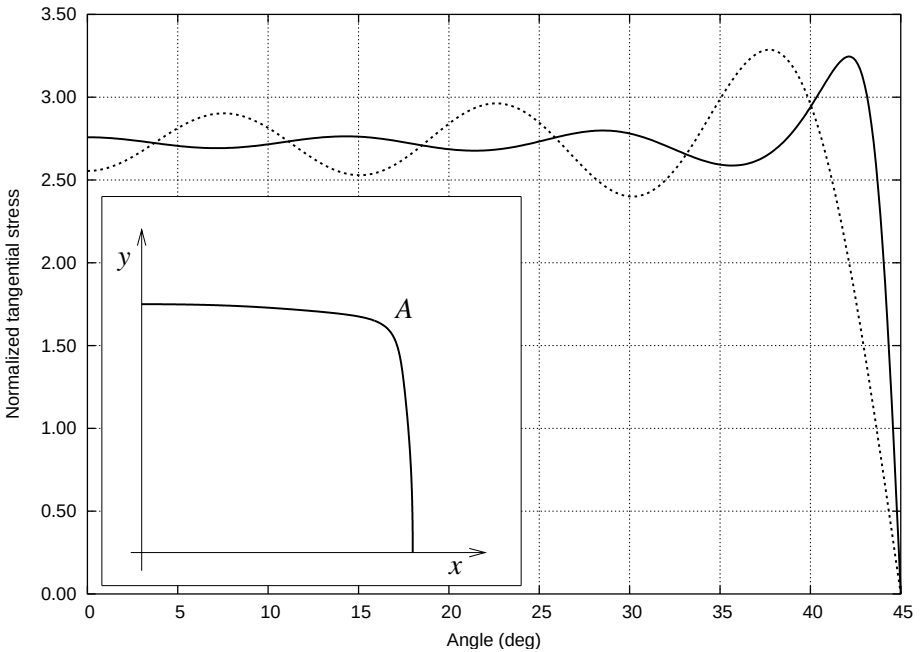

Figure 3. The tangential stress distribution along the δW-optimal hole shape (A) at $N = 23$: Exact summation (the solid line) versus truncation (the dotted line)

6. Analytical consequences of the main formula

In principle, the first N equations (16) with ease-to-compose coefficients can be solved analytically even for rather large N but we consider here only the simplest cases of one- and two-term mappings under pure shear ($B = 0,\ \Gamma = 1$).

One-term mapping. Let a hole with $(p+1)$-fold rotational symmetry ($p \geq 1$) be mapped by the function $\omega(\zeta) = \zeta + d_p\zeta^{-p}$. At $N = p$, the resolving $N \times N$ system (16) reduces to one or two equations, with $R_N(\zeta)$ becoming a monomial or binomial, respectively. Indeed, with (18), (24) and (11), a little algebra applied to (16) yields the following formulas:

Two- and three-fold symmetry ($p = 1, 2$):

$$a_2 = 1, \quad \delta W_2 = \frac{4}{(1 - pd_p^2)}: \qquad \min_{d_p} \delta W_p = 4, \quad d_p^{(\min)} = 0, \tag{27a}$$

$$\sigma_{\theta\theta}(\xi) = 4\frac{\cos 2\theta - pd_p \cos(p-1)\theta}{1 - 2pd_p \cos(p+1)\theta + p^2 d_p^2}. \tag{27b}$$

Square symmetry ($p = 3$):

$$a_2 = \frac{1}{1 - d_3}, \ \delta W_3 = \frac{4}{(1 - d_3)(1 - 3d_3^2)}: \ \min_{d_3} \delta W_3 = \frac{9}{\sqrt{2}+1}, \ d_3^{(\min)} = \frac{1 - \sqrt{2}}{3},$$

$$\sigma_{\theta\theta}(\xi) = \frac{4(1 - 3d_3)\cos 2\theta}{(1 - d_3)(1 - 6d_3 \cos 4\theta + 9d_3^2).}$$

Higher symmetry ($p \geq 4$):

$$a_2 = \frac{1}{1 - (p-2)d_p^2}, \ a_{p-1} = \frac{d_p(p-2)}{1 - (p-2)d_p^2}, \ \delta W_p = \frac{4}{(1 - (p-2)d_p^2)(1 - pd_p^2)},$$

$$\min_{d_p} \delta W_p = 4, \quad d_p^{(\min)} = 0,$$

$$\sigma_{\theta\theta}(\xi) = 4\frac{a_2(\cos 2\theta - pd_p \cos(p-1)\theta) + a_{p-1}(\cos(p+2)\theta - pd_p \cos 2\theta)}{1 - 2pd_p \cos(p+1)\theta + p^2 d_p^2}.$$

Excepting the square-symmetric case $p = 3$, the energy minimizing hole under remote shear appears to be a circle with $\mathcal{K}\big(d_p^{(\min)}\big) = 4$. Most likely, this is true not only for the one-term approximation but in general too. For triangular ($p = 2$) and hexagonal ($p = 5$) symmetry this fact was conjectured by Torquato et al. [1998] and is verified in Section 8, where the physical reasons behind the specifics of the square-symmetric optimal hole are also discussed.

Next, the value $p = 3$ yields

$$\begin{aligned} \mathcal{K}\big(d_3^{(\min)}\big) &= \max_{\theta} \big|\sigma_{\theta\theta}\big(\xi, d_3^{(\min)}\big)\big| \\ &= \sigma_{\theta\theta}\big(\theta_0, d_3^{(\min)}\big) = \frac{4\alpha(1 - 3d_3^{(\min)})}{\big(1 - d_3^{(\min)}\big)\big((1 + 3d_3^{(\min)})^2 - 12\alpha^2 d_3^{(\min)}\big)}; \end{aligned} \tag{28}$$

$$\alpha = \sqrt{\tfrac{1}{2}(\sqrt{2} - 1)}, \quad \theta_0 = \tfrac{1}{2}\arccos\alpha.$$

Analytical optimization of $\mathcal{H}(d_p)$ over the mapping term d_p, though routine, is too lengthy. Numerical GA optimization is performed instead (see Section 8).

Further we note that for any p, the energy maximum invariably occurs on the map univalency bound (13)

$$\max_{d_p} d_p^{(\max)} = \frac{1}{p}; \quad \omega_p(\zeta) = \zeta + \frac{1}{p\zeta^{-p}}; \quad \delta W_p = \begin{cases} 8, & p = 2, \\ 9, & p = 3, \\ \dfrac{4p^3}{(p^2-p+2)(p-1)}, & p \geq 4. \end{cases} \tag{29}$$

Therefore, the "worst" (shear energy maximizing) single hole as mapped by one-term function (29) is the $(p+1)$-cusped hypocycloid shown in Section 8. It has $(p+1)$ entrant angles where the tangential stress $\sigma_{\theta\theta}(\xi)$ goes to infinity.

The multi-term worst shapes reveal more complex behavior, which is analyzed numerically and displayed graphically in Section 8.

Two-term mapping. Here, we focus only on the square-symmetric case with $p = 3$, when

$$\omega(\zeta) = \zeta + d_3\zeta^{-3} + d_7\zeta^{-7}.$$

Solving the 2×2 system of the first nontrivial equations (16) yields

$$a_2 = \frac{1}{1 - d_3 - 3d_3d_7 - 5d_7^2}, \quad a_6 = \frac{3d_3 + 5d_7}{1 - d_3 - 3d_3d_7 - 5d_7^2},$$
$$\delta W_3 = \frac{4}{(1 - d_3 - 3d_3d_7 - 5d_7^2)(1 - 3d_3^2 - 7d_7^2)}.$$

The routinely obtained δW_3-minimum conditions take the form

$$3d_3(3d_3 + 10d_7) = 7d_7(1 + 3d_7), \tag{30a}$$
$$6d_3(5d_7^2 + 3d_3d_7 + d_3 - 1) = (1 + 3d_3)(1 - 3d_3^2 - 7d_7^2). \tag{30b}$$

Together with more explicit analytics like (28) and (29), they serve as a benchmark to configure the GA scheme.

7. Testing and calibration of the optimization scheme

The numerical accuracy of the proposed algorithm has been verified by reproducing the δW-related results. They fully coincide with those obtained differently in [Cherkaev et al. 1998] (Table 1). The corresponding evolution of the optimal square-like shape with N is not shown here; see the same reference.

We mention that the design variables d_m, $m = 1, \ldots, N$, are encoded using a discrete n-bit procedure when each coefficient d_m is approximated in view of (6) only by 2^n separate values in the continuous search space $[-1/\sqrt{m}; 1/\sqrt{m}]$.

These values are decoded from a randomly generated integer $P \in [-2^{n-1}; 2^{n-1}]$ as $d_k P = P/(2^{n-1}\sqrt{m})$. The genes for different coefficients are concatenated into a binary string of length Nn, or *chromosome*, which encodes the shape to be evaluated. The constant-size chromosome group so formed is then randomly subject to bitwise crossover and mutations that lead the initial population to the global optimum.

In this context it is of interest to evaluate the GA accuracy in dependence on the number of bits n by comparing with the analytical relations (27a), (29), (30). The results are collected in Table 3. This validates the approach and allows us to calibrate the heuristic GA parameters involved, such as population size and mutation rate. Typical GA settings chosen for the further $\mathcal{K}$-optimizations are given in Table 4.

Relation	Two bytes (16 bits)	Four bytes (32 bits)
(27a)	$< 2.1 \times 10^{-11}$	$< 4.4 \times 10^{-18}$
(29), $p = 3$	$< 7.4 \times 10^{-8}$	$< 2.0 \times 10^{-14}$
(29), $p = 5$	$< 3.8 \times 10^{-9}$	$< 4.8 \times 10^{-15}$
(30a)	$< 4.1 \times 10^{-6}$	$< 5.7 \times 10^{-9}$
(30b)	$< 5.8 \times 10^{-5}$	$< 1.6 \times 10^{-8}$

Table 3. Absolute error produced by GA optimization in cases of known analytical identities: two-byte versus four-bytes encoding.

Gene	Integer $\in [-2^{31}, 2^{31}]$	Individual	Interface shape
Population size	800	Number of genes	6
Initial population	Random	Selection format	Tournament
Elitism	Four best individuals	Termination	1200 iterations
Crossover	1-point	with rate	0.90
Creep mutation	Randomly change a bit	with rate	0.35
Jump mutation	Add random integer ± 64	with rate	0.35

Table 4. Typical GA setup used in our $\mathcal{K}$-optimizations.

8. Numerical results

We now present numerical results of the proposed method for a more complicated $\mathcal{K}$-optimization. Figures 4 and 5 exhibit the N-related evolution of the optimal hole shape and associated stress distributions, respectively. Table 5 shows the optimal parameters in dependence on increasing N. Comparison with the corresponding columns in Tables 1 and 2 indicates that δW- and $\mathcal{K}$-optimizations give rather similar values of the energy increment, while the maximum stresses differ significantly

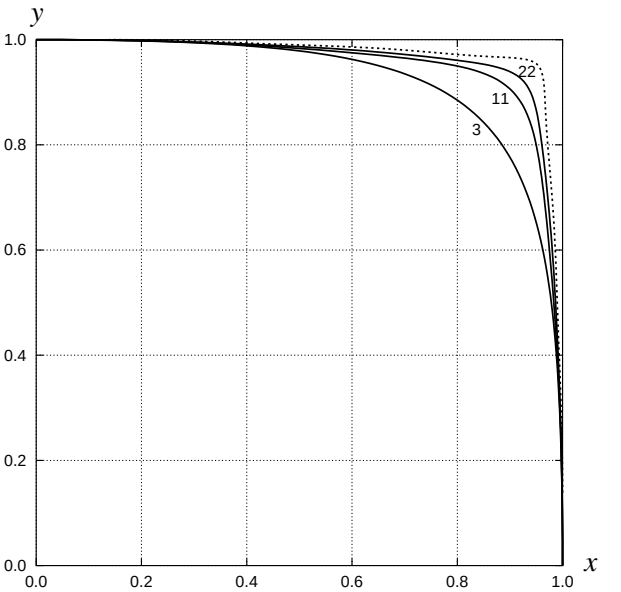

Figure 4. A quarter of the $\mathcal{H}$-optimal hole: evolution with increasing N ($N = 3, 11, 22$). The δW-optimal shape for $N = 23$ is added for comparison (dotted line).

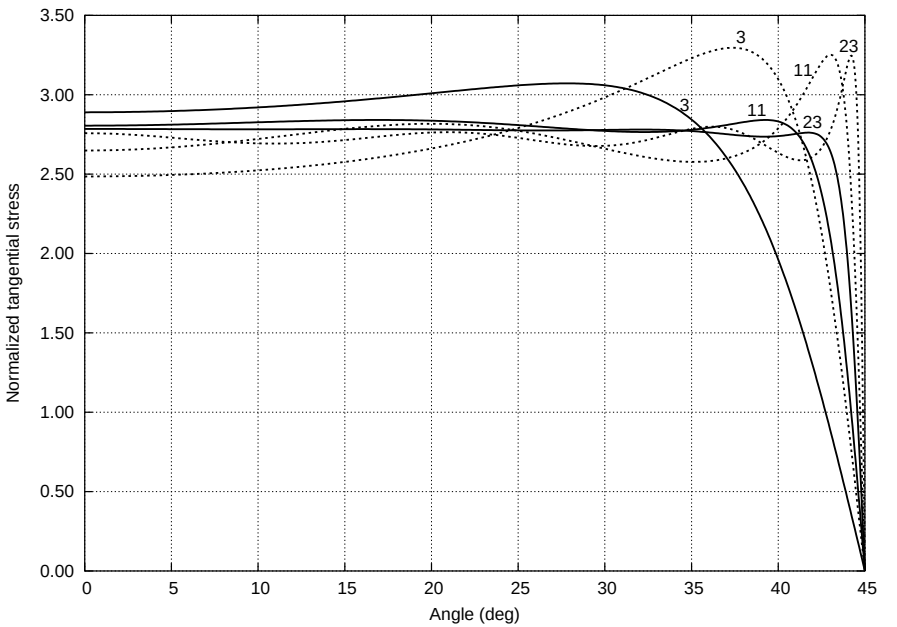

Figure 5. Tangential stress distribution along $\mathcal{H}$- and δW-optimal holes (solid and dotted lines, respectively) for $N = 3, 11, 23$.

N	d_3	d_7	d_{11}	d_{15}	d_{19}	d_{23}	$\mathcal{K}_{\min}$	δW
3	–0.09000						3.07165	3.76112
7	–0.11162	0.00751					2.90563	3.73211
11	–0.12182	0.01044	–0.00200				2.84110	3.72304
15	–0.12732	0.01210	–0.00293	0.00076			2.80824	3.71959
19	–0.13049	0.01293	–0.00340	0.00112	–0.00032		2.78843	3.71773
23	–0.13059	0.01292	–0.00338	0.00116	–0.00041	0.00010	2.77936	3.71770

Table 5. A single square-symmetric hole under remote shear: the conformal mapping coefficients and the local criterion $\mathcal{K}_{\min}$ resulted from the GA optimization process for different values of N. The corresponding global criterion δW is also shown to compare with its optimal values in Table 1.

(the relative discrepancies being respectively 0.086% and 16.8% at $N = 23$). However, close inspection of the stress distribution along optimal shapes of both types in Figure 5 shows that the discrepancy is concentrated near the forming angular point at $\theta = \pi/4$. In either case the stresses tend to obey the same identity (2). The different nature of the criteria defines the different convergence behavior of the optimal solutions: δW forms the angular point more rapidly, whereas the local $\mathcal{K}$-criterion allows no high-frequency peaks. This is clearly seen in Figure 4. With some caution, we conclude that both optimal solutions are the same, though an analytical proof would be very desirable. This is beyond our scope at the moment.

For triangular and hexagonal symmetry, similar computations lead to an interesting conclusion:

Under remote shear, the δW- and $\mathcal{K}$-optimal hole shape is a circle with $\delta W_{\min} = 4$ and $\mathcal{K}_{\min} = 4$.

In the absence of angular points, this has been verified with to extremely high accuracy.

The stress distribution along a circle is readily expressed as

$$\Phi_0(\zeta) = \Phi(\zeta) = \zeta^{-2}: \quad \sigma_{\theta\theta}(\xi) = 4\cos 2\theta, \quad \xi = \exp i\theta \in l,$$

(see [Muskhelishvili 1963]) with the sign-changing points lying on the bisectors of the quadrants

$$\theta = \frac{\pi(2j-1)}{4}, \quad j = 1, \dots, 4,$$

as in the square-symmetric case.

Geometrically, it is clear that other points location compatible with the remote shear antisymmetry may exist only for $(8p-4)$-symmetric shapes, $p = 2, 3, \dots,$

with an odd number of the points in a quadrant. However, GA optimization specially performed for $p = 2$ (dodecagonal symmetry) and $p = 3$ (icosagonal symmetry) bring us back to a circle.

Therefore, the prescribed square symmetry gives the only nontrivial example of the optimal shape where the angular points substantially reduce the values of both considered criteria as compared to a circle. The bottom row in Table 5 shows that $\Delta(\mathcal{K}) = 1 - 2.77936/4.0 = 30.5\%$ and $\Delta(\delta W) = 1 - 3.71449/4.0 = 7.1\%$.

Finally, the energy-maximization results are presented in Table 6 and Figure 6. At the first glance on the shapes it seems that the energy increment δW increases rapidly witn N due to the distinctive corner points which make finite contribution to the coefficient a_2 in (17). However, the most effective strategy really performed here by the GA is to minimize the hole area entering in (17) as a denominator. Indeed, as noted in the end of Section 3, finite-term mapping may not give a zero-area curve for $p \geq 2$. Therefore, as the only possible compromise between the finite number N of mapping terms and prohibited self-intersections the algorithm identifies the limiting case of the optimal shapes containing entrant angles that are of pure geometrical nature with no optimization resort. It is supported by the fact that the coefficient a_2 in Table 6 does not diminish with increasing N.

When N tends to infinity, the optimal mapping should then approximate a cross-like cut with $(p+1)$ equal arms as exemplified in Figure 6 for $p = 3$. This is the analitically known case [Ahlfors 1978] with

$$\omega(\zeta) = \zeta\left(1+\zeta^{-n}\right)^{2/n} = \zeta + \sum_{k=1}^{\infty} \frac{q(q-1)\ldots(q-k+1)\zeta^{-(p+1)k+1}}{k!}; \qquad q = \frac{1}{(p+1)}. \quad (31)$$

N	d_3	d_7	d_{11}	d_{15}	d_{19}	a_2	f_1/π	δW
1	0.33333					1.50000	0.66667	9.00000
2	0.42857	–0.14286				1.53139	0.30615	20.00833
3	0.43301	–0.14193	0.0631			1.56067	0.25450	24.52922
4	0.45091	–0.11683	0.0738	–0.0470		1.60610	0.20225	31.76542
5	0.46864	–0.11875	0.05391	–0.04401	0.02510	1.61902	0.16943	38.22265
∞	0.5	–0.125	0.0625	–0.03906	0.02734		0.0	∞

Table 6. A single square-symmetric hole under remote shear: the maximal mapping coefficients, the global criterion $\delta W_{\max}$ and its components a_2, f_1 found by the GA approach. The first row emerges analytically from (29) at $p = 3$. The last row contains the limiting data of the cross-like slit (31).

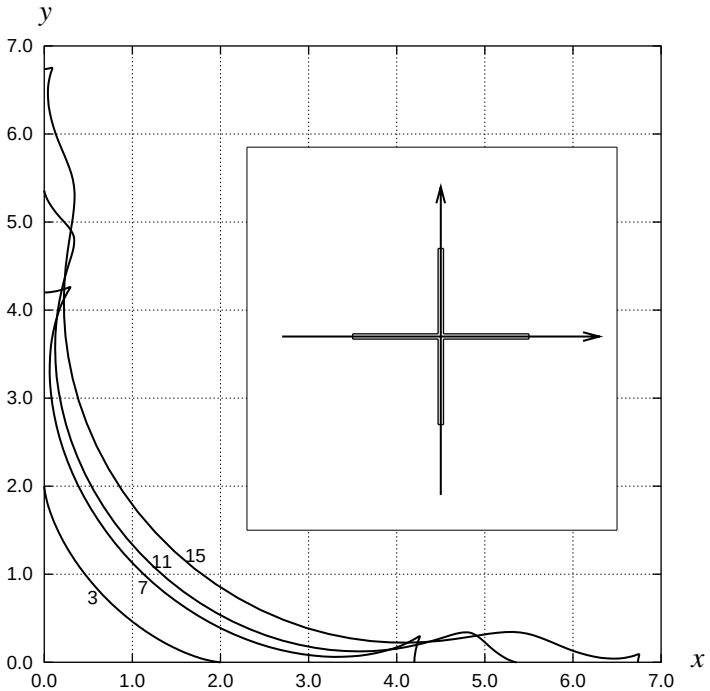

Figure 6. The energy-*maximizing* hole under square symmetry and remote shear: evolution to the limiting cross-like slit with increasing N. For $N = 3$ we have a four-cusped hypocycloid (29).

This reasoning is justified by the additional calculations in which the hole area was optimized instead of the energy. The resultant mapping terms practically coincide with those in Table 6. In turn, the latter converge, though slowly, to the cross-like limit (31).

9. Concluding remarks

The main goal of this work was to try a new GA scheme of shape optimization in plane elasticity when the conformal mapping is used instead of the direct nodal representation. In combination with the advanced fitness evaluation the proposed approach has enabled us to obtain new and significant results. This encoding may be also effective in other optimization problems governed by the conformal-invariant Laplace equation such as those in electrostatics. On the other hand, the current results are confined to the particular model with a single inhomogeneity. It is still unknown how this GA configuration will work in in the more realistic situation of multiple inclusions whose interaction hampers both the analytical and numerical manipulations. We hope to pursue this problem in further publications.

References

[Ahlfors 1978] L. V. Ahlfors, *Complex analysis: an introduction to the theory of analytic functions of one complex variable*, Third ed., McGraw-Hill, New York, 1978. MR 80c:30001

[Cherepanov 1974] G. P. Cherepanov, "Inverse problems of the plane theory of elasticity", *Prikl. Mat. Mekh.* **38**:6 (1974), 963–979. In Russian; translated in *J. Appl. Math. Mech.* **38**:6 (1974), 915–931. MR 52 #7254 Zbl 0315.73106

[Cherkaev et al. 1998] A. V. Cherkaev, Y. Grabovsky, A. B. Movchan, and S. K. Serkov, "The cavity of the optimal shape under the shear stresses", *Int. J. Solids Struct.* **35**:33 (1998), 4391–4410. MR 99e:73040

[Gen and Cheng 1997] M. Gen and R. Cheng, *Genetic algorithms and engineering design*, Wiley, New York, 1997.

[Holland 1975] J. H. Holland, *Adaptation in natural and artificial systems*, University of Michigan Press, Ann Arbor, MI, 1975. MR 55 #14256

[Kalandiya 1975] A. I. Kalandiya, *Mathematical methods of two-dimensional elasticity*, Mir Publishers, Moscow, 1975. MR 53 #4676

[Levy and Lessman 1958] H. Levy and F. Lessman, *Finite difference equations*, Pitman, London, 1958. Reprinted McMillan, New York, 1961, and Dover, New York, 1992. MR 21 #5827

[Movchan and Serkov 1997] A. B. Movchan and S. K. Serkov, "The Pólya–Szegő matrices in asymptotic models of dilute composites", *Eur. J. Appl. Math.* **8**:6 (1997), 595–621. MR 98m:73004

[Muskhelishvili 1963] N. I. Muskhelishvili, *Some basic problems of the mathematical theory of elasticity: Fundamental equations, plane theory of elasticity, torsion and bending*, 2nd English ed., Noordhoff, Groningen, 1963. Reprinted 1975; translated from the 4th Russian edition. MR 31 #920

[Pilkey 1997] W. D. Pilkey, *Peterson's stress concentration factors*, 2nd ed., Wiley, New York, 1997.

[Savin 1961] G. N. Savin, *Stress concentration around holes*, Pergamon, New York, 1961. MR 23 #B27

[Torquato 2002] S. Torquato, *Random heterogeneous materials*, Interdisciplinary Applied Mathematics **16**, Springer, New York, 2002. MR 2002k:82082

[Torquato et al. 1998] S. Torquato, L. V. Gibiansky, M. Silva, and L. Gibson, "Effective mechanical and transport properties of cellular solids", *Int. J. Mech. Sci.* **40**:1 (1998), 71–82.

[Vigdergauz 1976] S. B. Vigdergauz, "Integral equation of the inverse problem of the plane theory of elasticity", *Prikl. Mat. Mekh.* **40**:3 (1976), 566–569. In Russian; translated in *J. Appl. Math. Mech.* **40**:3 (1976), 518-522.

[Vigdergauz 2001a] S. B. Vigdergauz, "The effective properties of a perforated elastic plate: Numerical optimization by genetic algorithm", *Int. J. Solids Struct.* **38**:48-49 (2001), 8593–8616.

[Vigdergauz 2001b] S. B. Vigdergauz, "Genetic algorithm perspective to identify energy optimizing inclusions in an elastic plate", *Int. J. Solids Struct.* **38**:38-39 (2001), 6851–6867.

[Vigdergauz 2002] S. B. Vigdergauz, "Genetic algorithm optimization of the effective Young moduli in a perforated plate", *Struct. Multidiscip. O.* **24**:2 (2002), 106–117.

[Vigdergauz and Cherkayev 1986] S. B. Vigdergauz and A. V. Cherkayev, "A hole in a plate, optimal for its biaxial extension-compression", *Prikl. Mat. Mekh.* **50**:3 (1986), 524–528. In Russian; translated in *J. Appl. Math. Mech.* **50**:3 (1986), 401–404. MR 88g:73073 Zbl 0621.73022

Received 29 Sep 2005. Revised 16 Dec 2005.

SHMUEL VIGDERGAUZ: smuel@iec.co.il
R&D Division, The Israel Electric Corporation, Ltd., P.O.Box 10, Haifa 31000, Israel